Journal of NeuroVirology, 14: 102–118, 2008

ISSN: 1355-0284 print / 1538-2443 online
DOI: 10.1080/13550280701883832

informa
healthcare

Host strain-dependent difference in susceptibility in a rat model of herpes simplex type 1 encephalitis

Biborka Bereczky-Veress,[1] Olle Lidman,[2,*] Farideh Sabri,[1,*] Ivan Bednar,[3] Fredrik Granath,[4] Tomas Bergström,[6] Christian Spenger,[3] Alf Grandien,[5] Tomas Olsson,[2] Fredrik Piehl,[2] Margarita Diez,[2] and Birgit Sköldenberg[1]

[1]*Department of Medicine, Infectious Diseases Unit;* [2]*Department of Clinical Neuroscience, Neuroimmunology Unit;* [3]*Department of Clinical Science, Intervention and Technology;* [4]*Department of Medicine, Clinical Epidemiology Unit; and* [5]*Department of Medicine, Centre for Infectious Medicine, Karolinska Institutet, Stockholm, Sweden;* [6]*Department of Clinical Virology, Göteborg University, Göteborg, Sweden*

Herpes simplex encephalitis (HSE) is characterized by severe focal brain inflammation leading to substantial loss of nervous tissue. The authors established a model of *Herpes simplex* virus type 1 (HSV)-1–induced acute encephalitis in the rat by injecting into the whiskers' area a virus strain isolated from a fatal human HSE case. The model might resemble natural propagation of HSV-1 in humans; spreading from the mouth and lips via the trigeminal nerve to trigeminal ganglia and subsequently entering the central nervous system (CNS). HSV-1 infected Dark Agouti (DA) rats developed a well-synchronized disease and died 5 days after inoculation. HSV-1 detection by quantitative polymerase chain reaction (qPCR), virus isolation and immunohistochemistry, magnetic resonance imaging, and histopathological examination verified dramatic encephalitis mainly in the brainstem, but also in the olfactory bulb and other segments of the brain of diseased rats. In contrast, Piebald Virol Glaxo (PVG) rats were completely resistant to disease, displaying a more rapid clearance of peripheral infection and no evidence of virus entering into neither the trigeminal ganglia nor the CNS. These results suggest a regulation of susceptibility to HSV-1–induced encephalitis at the level of peripheral infection and subsequent neuronal uptake/transport of the virus. This provides a basis for future positioning of genetic polymorphisms regulating HSE and for dissection of important pathogenetic mechanisms of this severe human disease. *Journal of NeuroVirology* (2008) **14,** 102–118.

Keywords: apoptosis; CNS infection; encephalitis; *Herpes simplex*; inbred rat strains; inflammation

Introduction

Herpes simplex virus type 1 (HSV-1) encephalitis (HSE) is a rare human disease, affecting 2 to 4 individuals/million/year, although the virus infects a high percentage of the population and often persists lifelong in the trigeminal ganglia. HSV-1 is a neurotropic virus with the ability to infect the central nervous system (CNS), to replicate in neurons and glia cells, and to subsequently produce acute focal,

Address correspondence to Biborka Bereczky-Veress, Karolinska Institutet, Department of Medicine, Infectious Diseases Unit, CNS Group, Karolinska University Hospital, CMM, L8:01, SE-171 76 Stockholm, Sweden. E-mail: biborka.bveress@ki.se

*Olle Lidman and Farideh Sabri contributed equally to this work.

This work was supported by 6th Framework Program of the European Union, NeuroproMiSe, LSHM-CT-2005-018637, and the EURATools, LSHG-CT-2005-019015, as well as by grants from the Wadsworth Foundation, Torsten and Ragnar Söderbergs Foundation, The Foundation for the Memory of Sigurd and Elsa Golje, Hjärnfonden, The Swedish Society for Medical Research, Björklunds Foundation, Nils and Bibbi Jenssens Foundation, Montel Williams Foundation, Magnus Bergvalls Foundation, Swedish Science Council, and The Swedish Association of Persons with Neurologically Disabilities. The authors would like to thank Maria Johansson for skilled work with the virological analyses and the employees at the Astrid Fagræus laboratory of the Swedish Institute for Infectious Disease Control for taking excellent care of the rats. The experimental MRI unit is a core facility supported by Karolinska University Hospital and Karolinska Institutet.

Received 29 May 2007; revised 26 October 2007; accepted 26 November 2007.

necrotizing encephalitis (Booss and Kim, 1984). HSE is the most common cause of nonepidemic, acute fatal encephalitis in the western world (Sköldenberg, 1991) and has a tendency to relapse or to have a progressive course (Sköldenberg *et al*, 2006). Despite antiviral treatment with acyclovir, HSE remains a very severe medical condition, with a mortality rate of about 20% and with considerable neurological deficits in individuals surviving the acute phase (Sköldenberg *et al*, 1984; Whitley *et al*, 1986). Immunological studies in HSE demonstrate widespread glial activation and presence of markers for immune activation and for brain tissue destruction in the cerebrospinal fluid (CSF) (Studahl *et al*, 2000). In addition, persistently increased levels of sFas and sCD8 can be detected in CSF (Aurelius *et al*, 1993, 1994 Sabri *et al*, 2006; Sköldenberg *et al*, 2006). The mechanisms underlying the pathogenesis and the genetic susceptibility are largely unknown. However, a recent study identified a deficiency in UNC-93B protein, linked to impaired interferon-α/β and -λ antiviral responses, as a susceptibility factor for HSE in children (Casrouge *et al*, 2006).

The aim of the present study was to set up a rat model for human HSE, to examine the interaction between a neurovirulent strain of HSV- 1 and the CNS, as well as to study if the genetic background influences the susceptibility to HSE. By injecting HSV-1 subcutaneously (s.c.) into the whiskers' area of two inbred rat strains, Dark Agouti (DA) and Piebald Virol Glaxo (PVG), previously known to differ in their vulnerability to autoimmune neuroinflammation and in their response to nerve injury (Holmdahl *et al*, 1985; Lidman *et al*, 2003; Lorentzen *et al*, 1997; Lundberg *et al*, 2001; Weissert *et al*, 1998), we created a novel rat model of acute HSE. The results obtained in this study suggest a regulation of susceptibility to HSE at the level of clearance of peripheral infection and/or neuronal uptake/transport of the virus.

Results

Clinical disease

Forty-five-day-old male DA and PVG rats were injected subcutaneously in the right whiskers' area with 2×10^6 plaque-forming units (PFU) of human brain biopsy-derived HSV-1 (strain I-2762). None of the animals showed clinical signs of disease before 5 days post inoculation (d.p.i.). The first clinical signs of disease were observed in the morning of day 5 post inoculation, the DA rats exhibited unsteady posture, and later on a tendency for counter clockwise rotator movements. Within 3 to 5 hours after the appearance of the first symptoms, the psychomotor behavior deteriorated with development of hind limb paralysis starting on the right side. In addition, diseased DA rats displayed porphyry around the nostrils and on the interior side of the front limbs as a result of grooming, profuse salivation, aggressive behavior, considerable weight loss (approximately 18% compared to the body weight measured at 4 d.p.i.), and thereafter death. Unless euthanized, the mortality in this group of animals was 100%. In contrast, PVG rats showed no symptoms during the entire experiment. In preliminary titration experiments, even higher doses (5×10^6 PFU) of HSV-1 also failed to induce disease in PVG rats within 6 months after inoculation (data not shown). In young adult DA and PVG rats injected with 2×10^6 PFU HSV-1, susceptibility to HSE is neither sex, nor body weight, only strain dependent.

Magnetic resonance imaging

T2-weighted RARE (rapid acquisition with relaxation enhancement) images recorded at 1, 3, and 5 d.p.i. were compared to images recorded one day prior to inoculation (day −1) on the same rats. In DA rats, MRI detected pathological changes consistent with substantial edema at the level of the trigeminal nuclei in the brainstem on the ipsilateral side at 5 d.p.i. No pathological signs were evident in DA rats at earlier time points, or in PVG rats at any time point (Figure 1).

Propagation of virus

Quantitative real-time polymerase chain reaction (qPCR) was used to assess HSV-1 DNA and demonstrated 10^4 to 10^6copy numbers of HSV-1 at the site of inoculation in the skin of whiskers' area in both DA and PVG rats at 5 d.p.i. However, higher titers were found in the whiskers' area on the ipsilateral side of the DA rat compared to the PVG rat ($P = .22$) (Figure 2a). No virus DNA could be detected on the contralateral side, except for a few copies in some of the duplicate measurements (Figure 2a). In the trigeminal ganglia, brainstem, cerebellum, thalamus, cortex, and olfactory bulb of DA rats, copy numbers of about 10^6 to 10^8were detected. Except for a few samples positive at low copy numbers (10^2 to 10^3), all examined brain regions from PVG rats were negative (Figure 2a).

As an additional measure, HSV-1 titers in brainstem and thalamus of inoculated rats were assessed by virus isolation in GMK-AH1 cell cultures (Figure 2b). This method demonstrated similar results, with high titers of virus ($\geq 10^5$ PFU/ml) in all samples from DA rats, whereas no detectable virus was retrieved in PVG rats. Interestingly, virus isolation attempts from whiskers' area at 5 d.p.i. were negative in both DA and PVG rats (Figure 2b).

In a subsequent experiment we studied the kinetic pattern of HSV-1 propagation using samples from the whiskers area, the trigeminal ganglia and the brainstem at 12, 24, 48, 72, 96, and 120 h post inoculation (p.i.) in three DA and three PVG rats at each time point. These samples were later analyzed by qPCR as well as by virus isolation in GMK-AH1 cells. HSV-1 DNA was detectable by qPCR in the whiskers area of both PVG and DA rats on the ipsilateral side,

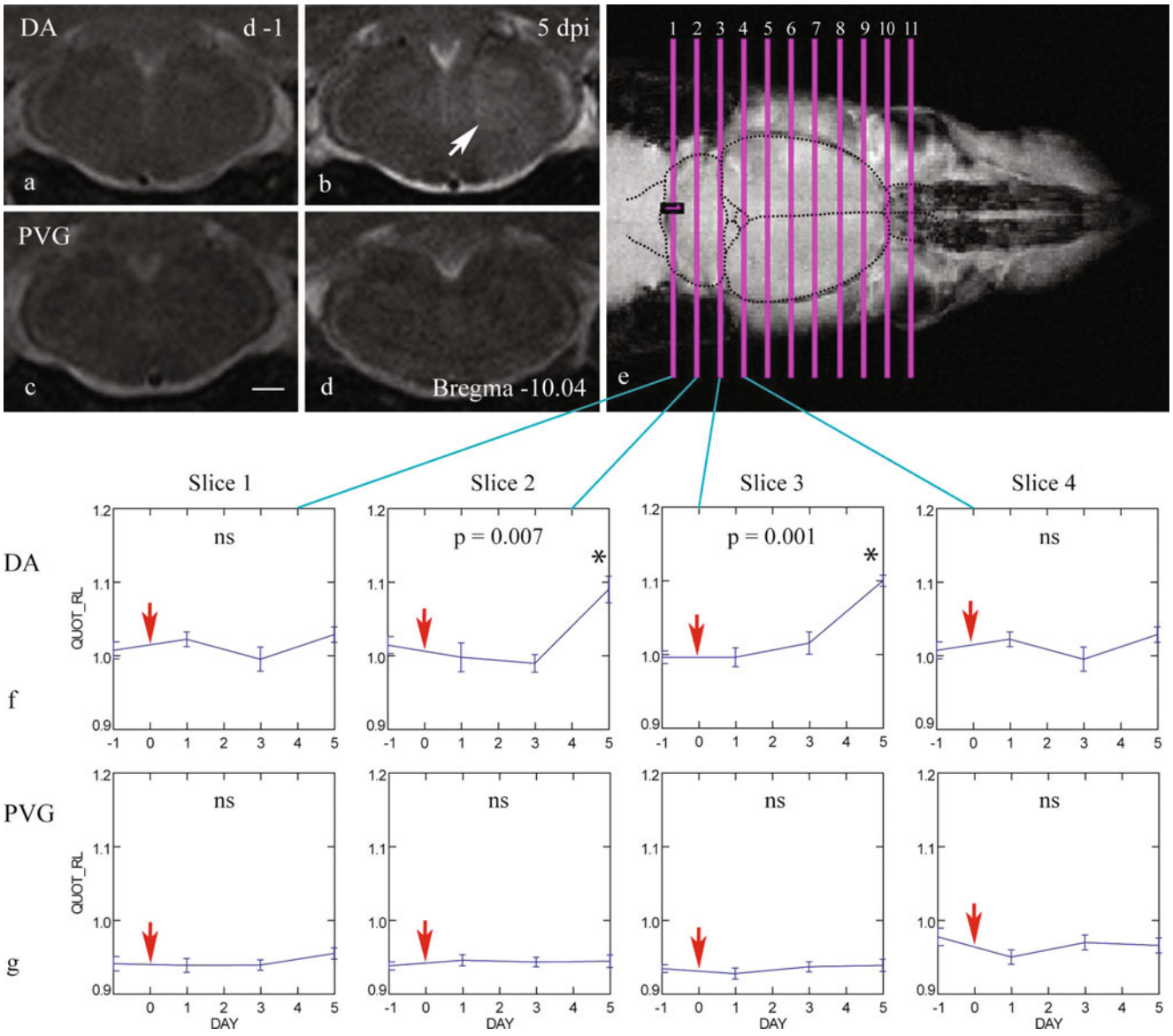

Figure 1 HSV-1 infection causes edema in the brainstem of DA rats. Magnetic resonance imaging of the brainstem (slice 2) of DA (**a**, **b**) and PVG (**c**, **d**) rats prior to HSV-1 inoculation (**a**, **c**), and at 5 d.p.i. (**b**, **d**), respectively. White arrow (**b**) indicates edematous area on the ipsilateral side of the brainstem in a DA rat; (**e**) the caudorostral positioning of the 11 MRI slices; (**f**) quantification of the MRI signal reveal changes consistent with development of edema in the brainstem at the level of the trigeminal nuclei (slice 2 and 3) in DA rats between 3 and 5 d.p.i.; (**g**) no such changes are evident in PVG rats. Red arrows in (**f**) and (**g**) indicate the time point of HSV-1 inoculation. Scale bar = 1 mm.

predominantly during the first 24 h p.i. but in lower numbers throughout the study period (Figure 3a). This is consistent with partial clearance of HSV-1 in both DA and PVG rats at the inoculation site.

No HSV-1 DNA could be demonstrated in the trigeminal ganglia or the brainstem of the PVG rats. In contrast, in the trigeminal ganglia of the DA rats, low copy numbers of HSV-1 DNA were found at 12 and 24 h p.i. and high copy numbers (10^5) from 48 h p.i. In the brainstem of the DA rats, high copy numbers of HSV-1 DNA could be demonstrated at 72 h p.i. and was present even at later time points (Figure 3a).

HSV-1 could be isolated from the whiskers' area at the ipsilateral side of PVG rats at 12 to 24 h p.i. (10^2 to 10^3 PFU), meanwhile in the DA rats, the persistence of HSV-1 was longer (12 to 96 h), and higher quantities (10^4 to 10^5 PFU) of virus could be detected. HSV-1 could not be isolated from the trigeminal ganglia or the brainstem of the PVG rats in contrast to the corresponding areas in DA rats from which HSV-1 was isolated already from 48 h p.i. (Figure 3b).

Virus propagation in the brain was studied by immunohistochemical staining for HSV-1 (Figure 4a to k). HSV-1 immunoreactivity was only detected in DA rats. The first HSV-1 immunoreactive cells appeared at 2 d.p.i. on the ipsilateral side in the ventrolateral part of the brainstem in the spinotrigeminal

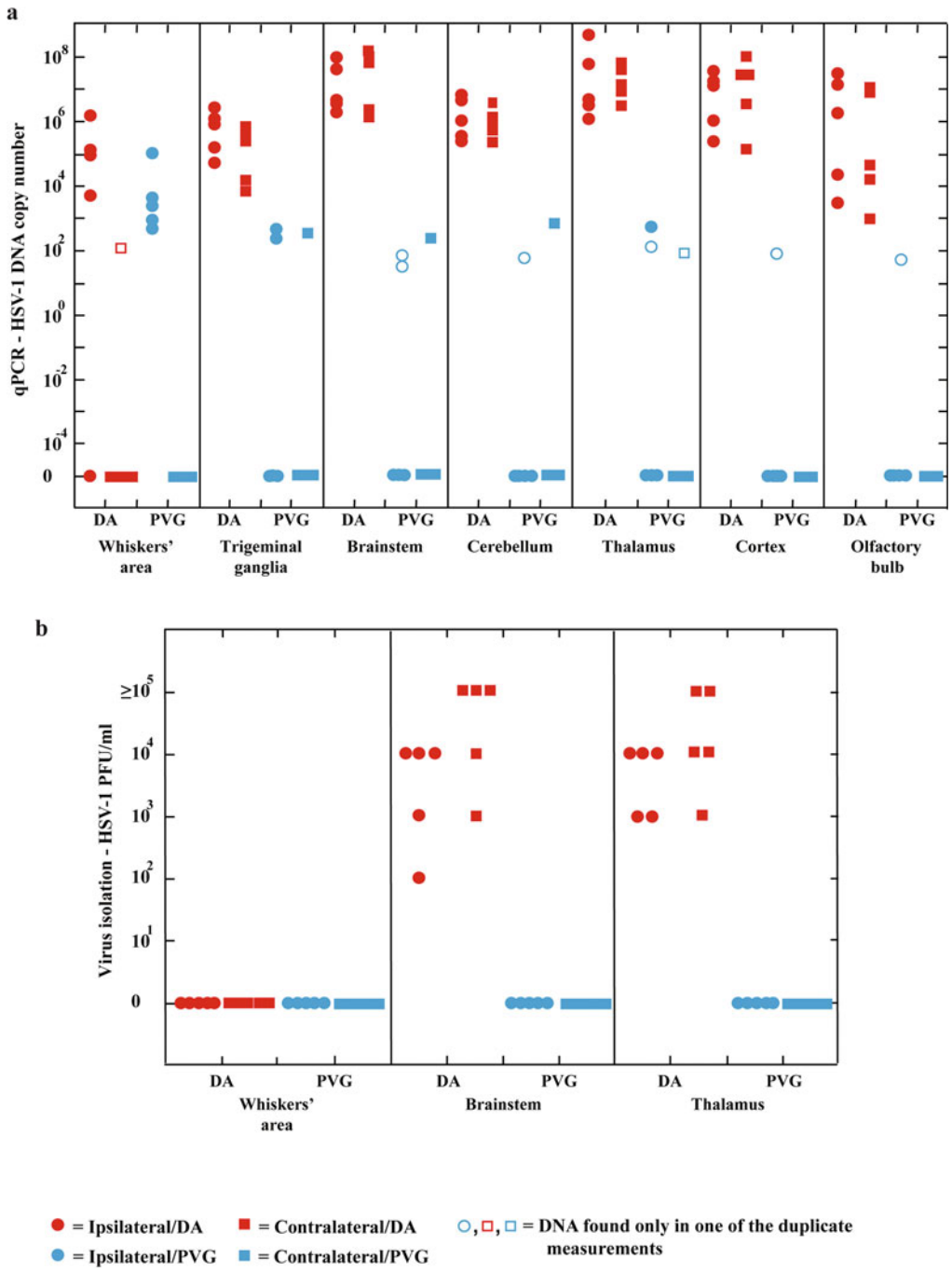

Figure 2 Differences between HSV-1 levels in DA and PVG rats revealed by qPCR (**a**) and virus isolation (**b**) in the whiskers' area, trigeminal ganglia and brain at 5 d.p.i. (**a**) qPCR measurements of HSV-1 DNA (logarithmic scale) in the whiskers' area, trigeminal ganglia and in various brain regions in DA and PVG rats at 5 d.p.i. The results reveal different levels of clearance of HSV-1 in the whiskers' area between the two rat strains. In all areas of measurement DA shows significantly higher number of DNA copies than PVG ($P < .01$) except for the whiskers' area. No significant differences between ipsilateral and contralateral measurements can be detected. (**b**) Virus titers in whiskers's area, brainstem, and thalamus measured in GMK-AH1 cell cultures (logarithmic scale). No virus could be retrieved from the whiskers' area of DA and PVG rats. However, in the brainstem and thalamus high virus titers were present in all examined DA rats at 5 d.p.i., whereas all PVG samples were negative. In brainstem and thalamus DA presents significantly higher viral load compared to PVG ($P < .01$), but not in the whiskers' area. No significant differences can be detected between the ipsilateral and the contralateral side.

tract and in the root of the facial nerve (Figure 4e). At 3 d.p.i., larger HSV-1 immunopositive infiltrates were present (Figure 4a, f). These were composed of cells as well as a diffuse pattern visible in the surrounding tissue, probably reflecting leakage of viral particles from cells into the extracellular compartment. At 4 d.p.i., HSV-1 labeling was detected also on the contralateral side of the brainstem (Figure 4b,

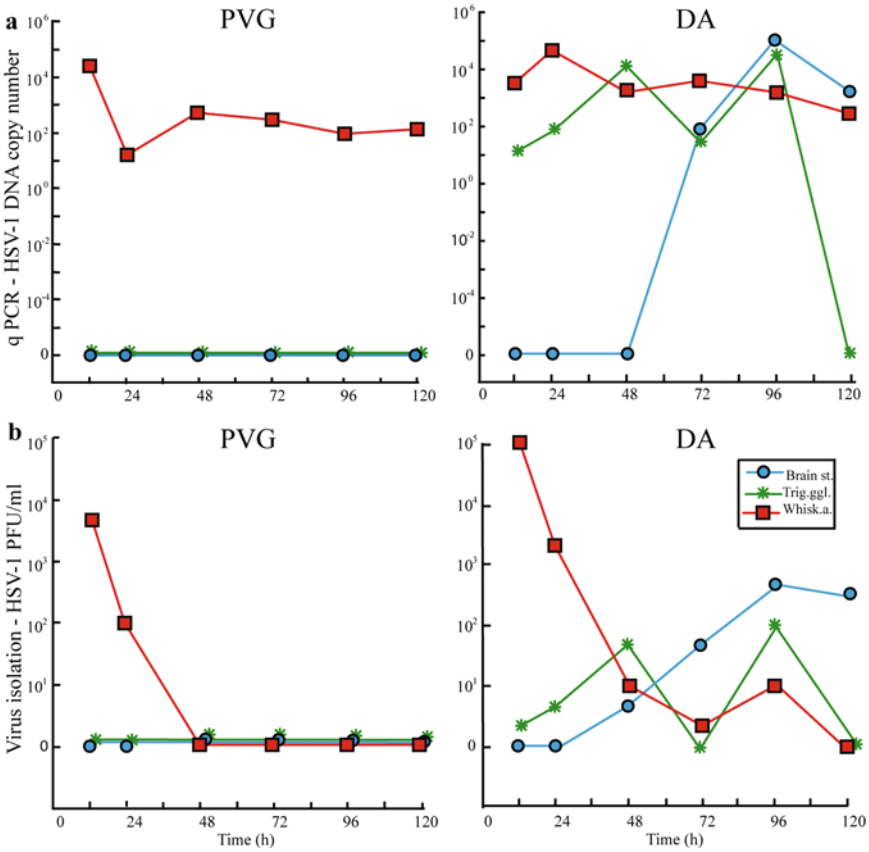

Figure 3 Kinetic studies of HSV-1 levels assessed by qPCR (**a**) and HSV-1 isolation (**b**) in the whiskers' area, trigeminal ganglia, and brainstem reveal differences between DA and PVG rats. (**a**) In the whiskers' area, mean values of HSV-1 copy numbers are high in both rat strains. However, the levels of HSV-1 DNA copies in the whiskers' area are not significantly different over time in any of the strains, nor compared between DA and PVG rats. In the trigeminal ganglia of the DA rats, elevated levels are detected already from 12 h pi. The HSV-1 DNA levels are significantly higher in DA compared to PVG rats ($P < .001$) at all time points (**a**), but no significant difference can be detected over time. In PVG rats, no HSV-1 DNA is detected. In the brainstem of the DA rats elevated levels of HSV-1 DNA can be seen after 48 h pi. The HSV-1 DNA levels vary significantly different over time ($P < .001$), whereas no HSV-1 DNA levels are detected in the PVG rats at any time point. (**b**) Virus isolation from the whiskers' area reveals decreasing levels of HSV-1 from 12 h pi in both strains. The viral load is found to be significantly higher in DA compared to PVG rats over time ($P < .001$). Virus is cleared from the whiskers' area of the PVG rats after 48 h pi, but in the DA rats it persists at low levels. In the trigeminal ganglia higher viral load can be found in DA compared to PVG rats ($P < .05$), but no significant difference in time dynamics can be seen. In the brainstem, increasing levels are demonstrated in the DA rats after 24 h pi, whereas no virus can be isolated from the PVG rats at any time point. The time dynamics of the viral load is significantly different between DA and PVG rats ($P < .001$).

g). Finally, at 5 d.p.i., a diffuse HSV-1 labeling covered the entire cross-section of the brainstem on both ipsi- and contralateral sides (Figure 4c, h). At this point, several HSV-1 immunopositive foci were present also in the cerebellum (Figure 4j). In the thalamus, a few immunopositive foci, mostly on the contralateral side were observed at 4 d.p.i., increasing in number at 5 d.p.i. (Figure 4k), whereas the hippocampus remained negative. Sections taken at the level of the frontal cortex and the olfactorial bulbs did not stain for HSV-1 at any time point. No HSV-1 immunoreactivity was observed in control DA (Figure 4d), control PVG, or HSV-1–infected PVG rats (Figure 4i) at any level or time point studied. HSV-1 labeling was completely abolished after preabsorbtion of the antibody with HSV-1 prior to staining confirming the specificity of the antibody (Figure 4l).

Host response

The host response was studied using immunohistochemistry for major histocompatibility complex (MHC) class II (mainly expressed on activated microglia) and the astrocyte marker glial fibrillary acid protein (GFAP). A few scattered MHC class II–positive cells were present in control DA (Figure 5a), but not in PVG rats. A discrete increase in MHC class II labeling was detected in the ipsilateral trigeminal nuclei of inoculated DA rats at 2 d.p.i. One day later, at 3 d.p.i., large numbers of MHC class II–positive cells were present in the brainstem on the ipsilateral side (Figure 5b). By 4 d.p.i., MHC class II labeling was present on both sides of the brainstem (Figure 5c), and the labeling intensity had increased further at 5 d.p.i. (Figure 5d). MHC class II–positive cells were detected in cerebellum from 5 d.p.i. (Figure 5e) and in thalamus already from 3 d.p.i. As can be seen

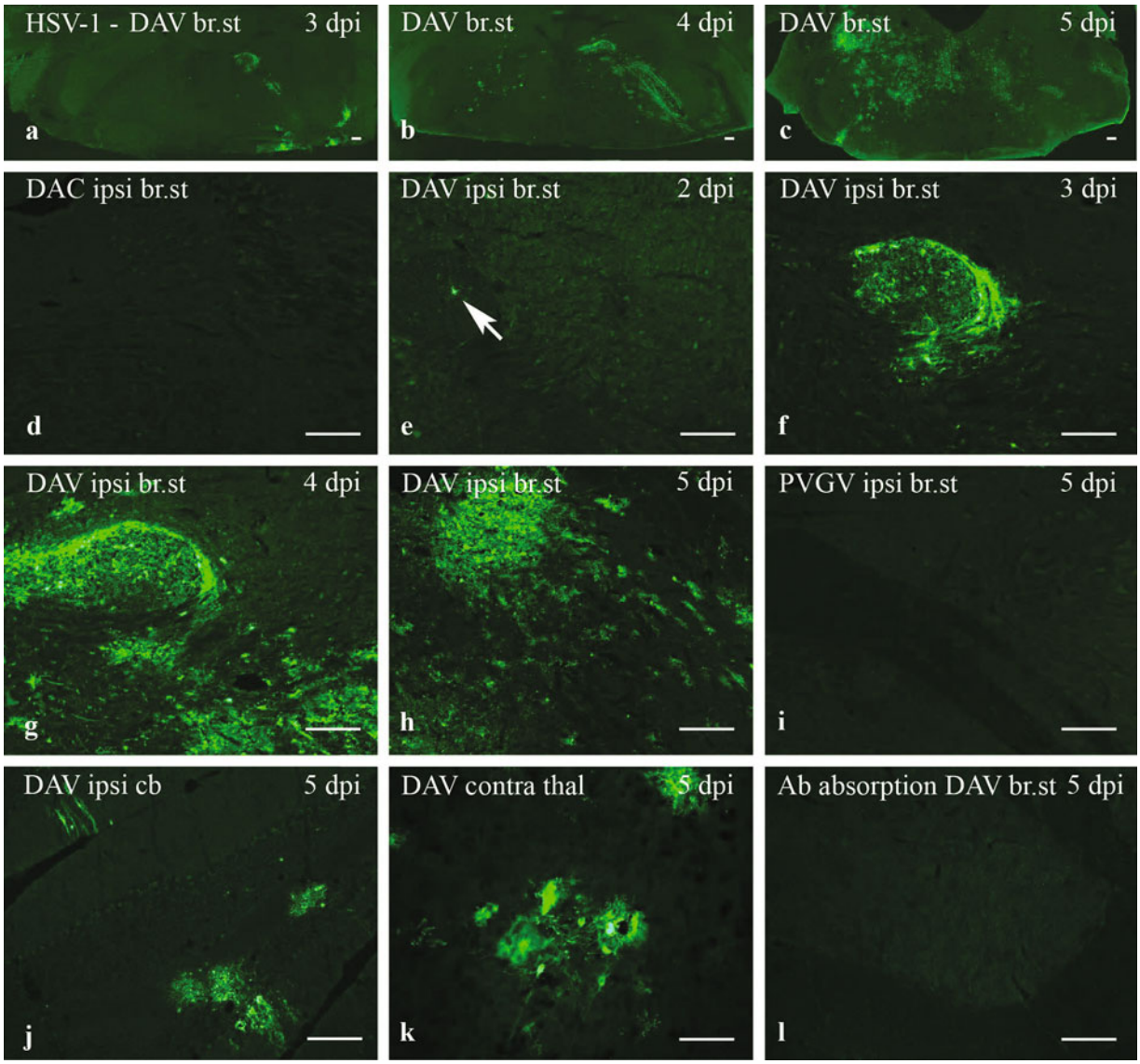

Figure 4 HSV-1 immunoreactivity is detected in the CNS of DA, but not PVG, rats. Kinetics of HSV-1 infectious propagation visualized with HSV-1 immunoreactivity: (**a**) Low-magnification micrograph of brainstem section from a DA rat at 3 d.p.i. with distinct staining in the area of trigeminal nuclei and the facial nerve tract on the ipsilateral side; (**b**) by 4 d.p.i. there is further spreading of virus on the ipsilateral side together with the appearance of focal staining on the contralateral side; (**c**) overview of the brainstem in a DA rat at 5 d.p.i., displaying HSV-1 immunoreactivity on both sides, but with highest intensity on the contralateral side; (**d**) HSV-1 immunoreactivity is absent in the brainstem of a control DA rat; (**e**) a single immunopositive cell on the ipsilateral side of the brainstem in a DA rat at 2 d.p.i.; (**f**) immunopositive neuronal cell bodies and surrounding amorphous labeling in the brainstem of a DA rat at 4 d.p.i.; (**g**) maximum labeling on the ipsilateral side in DA rats is reached at 4 d.p.i.; (**h**) at day 5, labeling in the brainstem is more diffuse, but with less intensity on the ipsilateral side, suggesting clearance of virus; (**i**) complete lack of HSV-1 immunoreactivity in the brainstem of a PVG rat at 5 d.p.i.; (**j**) immunoreactive cells in the cerebellum of a DA rat at 5 d.p.i.; (**k**) immunoreactive cells in the contralateral side of the thalamus of a DA rat at 5 d.p.i.; (**l**) no immunoreactivity for HSV-1 is present in the brainstem of a DA rat at 5 d.p.i. after preabsorption of the antibody with HSV-1. Scale bar = 200 μm.

from Table 1, MHC class II, ED1, as well as CD8 immunoreactivity was also present in the olfactory bulb and other areas of DA rats. No increase of these markers was detected in HSV-1–infected PVG rats (Figure 5f).

GFAP-positive astrocytes were observed in both control DA (Figure 5g, j) and PVG rats. A slight increase in GFAP labeling was present in the brainstem of diseased DA rats from 4 d.p.i. At 5 d.p.i., GFAP labeling was clearly increased in infected DA rats (Figure 5h, k) compared both to control DA (Figure 5g, j) and to HSV-1–infected PVG rats (Figure 5i, l). Hematoxylin and eosin (H&E) staining revealed mononuclear cell infiltrates only in diseased DA rats (Figure 6). Cellular infiltrates started to appear around blood vessels in the brainstem on the ipsilateral side at 3 d.p.i., with further progressing and spreading to the contraletaral side by 4 d.p.i. (Figure 6c, d). Brainstem sections from DA rats at 5 d.p.i. revealed massive inflammatory infiltrates

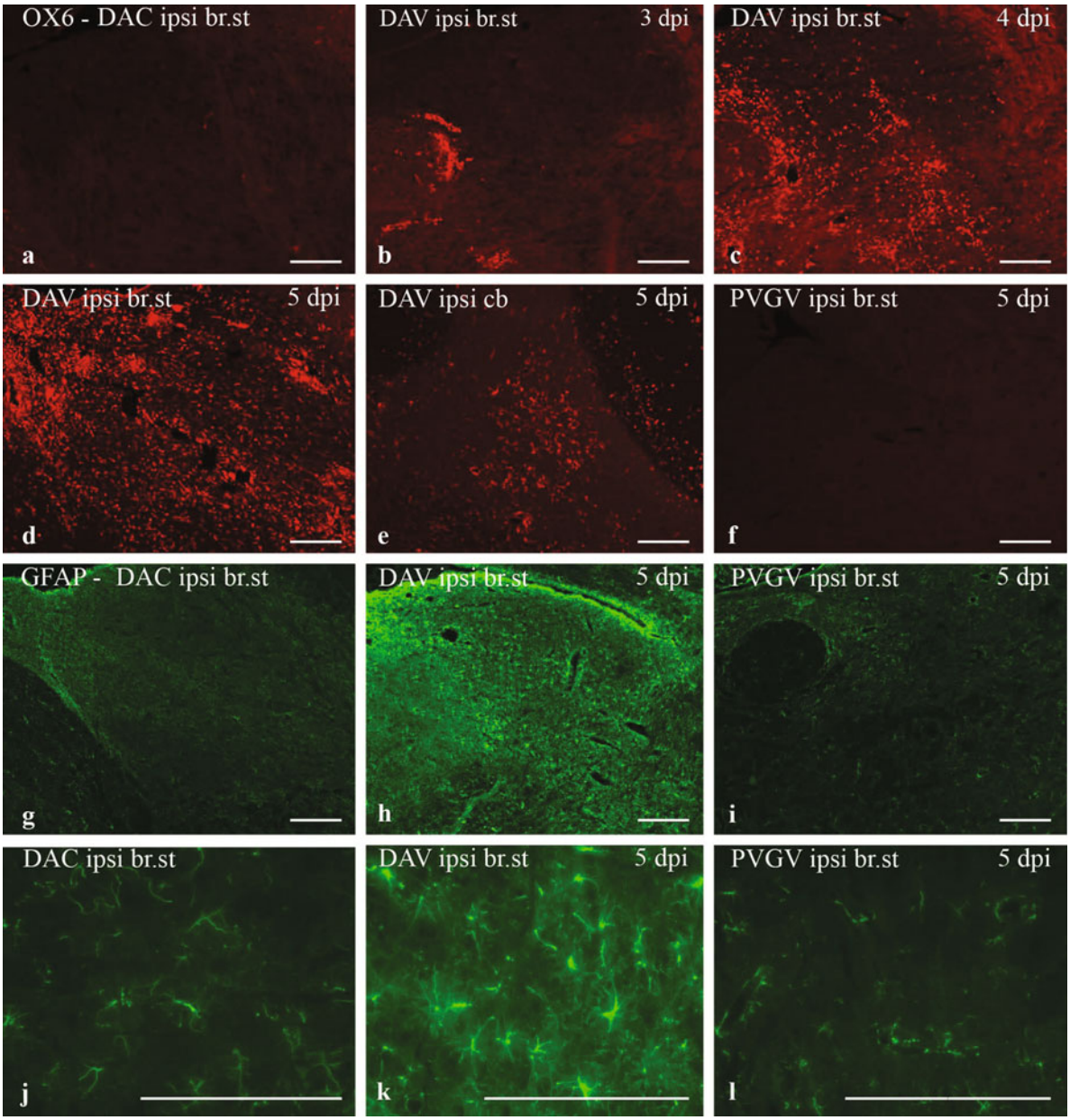

Figure 5 Intense activation of resident glial cells in the CNS of DA rats after HSV-1 infection. Host tissue reaction as a consequence of HSV-1 infection visualized by immunofluorescence labeling for OX-6 (MHC class II expressed mainly on activated microglia) and GFAP (astrocytes): (**a**) There is an almost complete lack of OX-6–positive cells in the brainstem of control DA rat; (**b**) OX-6–positive cell clusters first appear on the ipsilateral side of the brainstem in a DA rat at 3 d.p.i.; (**c**) a rapid increase in the number of OX-6–positive cells in the brainstem is evident by 4 d.p.i.; (**d**) at 5 d.p.i., in the DA rat, there is massive OX-6 labeling in the brainstem parenchyma; (**e**) in DA rats at 5 d.p.i., clusters of OX-6–positive cells are also present in the cerebellum; (**f**) brainstem section from a PVG rat at 5 d.p.i. devoid of OX-6 labeling; (**g**) GFAP labeling of astrocytes in the brainstem of a control DA rat; (**h**) a more intense and confluent pattern of GFAP labeling is present on the ipsilateral side of the brainstem in a DA rat at 5 d.p.i.; (**i**) weak labeling of GFAP-positive astrocytes in a PVG rat at 5 d.p.i.; (**j**) resting astrocytes in the brainstem of a control DA rat; (**k**) activated, hypertrophic GFAP-positive astrocytes in the brainstem of a DA rat at 5 d.p.i.; (**l**) GFAP-positive cells in the brainstem of a PVG rat at 5 d.p.i. without discernible signs of activation. Scale bar = 200 μm.

throughout the tissue (Figure 6e, f). In addition, at this time point, perivascular infiltrates were detected also in the cerebellum and the thalamus (Table 1).

The ED1 antibody, labeling microglia-/monocyte-derived phagocyting cells (Dijkstra *et al*, 1985), showed occasional positive cells in proximity to blood vessels in control DA rats (Figure 7a). ED1-positive cells first appeared on the ipsilateral side in the brainstem of DA rats 2 d.p.i. and rapidly increased in numbers during the following days (Figure 7b to d). Positive cells were present also in the thalamus, mainly on the contralateral side (Figure 7e), and in the cerebellum at later stages of infection. Baseline

Table 1 HSV-1 infection causes alteration of specific markers in the brain of DA but not in the PVG rats

Marker	Rat strain	Day post infection	Brainstem, cerebellum	Thalamus	Cortex, striatum	Olfactory bulb*
HSV-1	DA	Control	−	−	−	−
		1	−	−	−	−
		2	+	−	−	−
		3	++	−	−	−
		4	+++	++	−	−
		5	+++++	+++	+	−
	PVG	5/control	−	−	−	−
OX6	DA	Control	+	+	+	+
		1	+	+	+	+
		2	++	++	+	++
		3	+++	+++	+	++
		4	+++	+++	+	++
		5	+++++	+++	+	+++
	PVG	5/control	−	−	−	−
GFAP	DA	Control	+	+	+	+
		1	+	+	+	+
		2	+	+	+	+
		3	++	+	+	+
		4	++	++	+	++
		5	+++	++	+	++
	PVG	5/control	+	+	+	+
ED1	DA	Control	+	+	+	+
		1	+	+	+	+
		2	++	+	+	+
		3	+++	+	+	++
		4	+++	++	+	++
		5	+++	+++	+	+++
	PVG	5/control	++	++	++	++
CD4	DA	Control	−	−	−	+
		1	−	−	−	+
		2	−	−	−	+
		3	++	−	−	+
		4	+++	+	−	+
		5	+++	++	−	+
	PVG	5/control	−	−	−	+
CD8	DA	Control	−	−	−	−
		1	−	−	−	−
		2	−	−	−	+
		3	++	−	−	+
		4	++	−	−	+
		5	+++	+	−	++
	PVG	5/control	−	−	−	−
NKR	DA	Control	−	−	−	+
		1	−	−	−	+
		2	−	−	−	+
		3	++	−	−	+
		4	+++	+	−	+
		5	+++	++	−	+
	PVG	5/control	−	−	−	−
TUNEL	DA	Control	−	−	−	−
		1	−	−	−	−
		2	−	−	−	−
		3	+	−	+	+
		4	+++	+	−	+
		5	+++	++	+	+
	PVG	5/control	−	−	−	+
H&E	DA	Control	−	−	−	−
		1	−	−	−	−
		2	−	−	−	−
		3	+	−	−	−
		4	+++	+	−	−
		5	+++	++	−	−
	PVG	5/control	−	−	−	−

Note. The immunopathology of the brain at days 1 to 5 after s.c. HSV-1 injection in susceptible DA rats ($n = 15$) compared to HSV-1–infected resistant PVG rats ($n = 15$), and DA ($n = 10$) and PVG ($n = 10$) controls.
+ = the first visible sign of staining**; ++ = staining present on one side**; +++ = staining spread on one side and signs on the opposite side**; ++++ = staining spread on both sides; +++++ = massive labeling on both sides.
*Both ipsi- and contralateral sides; **ipsilateral in the brainstem and contralateral in the thalamus.

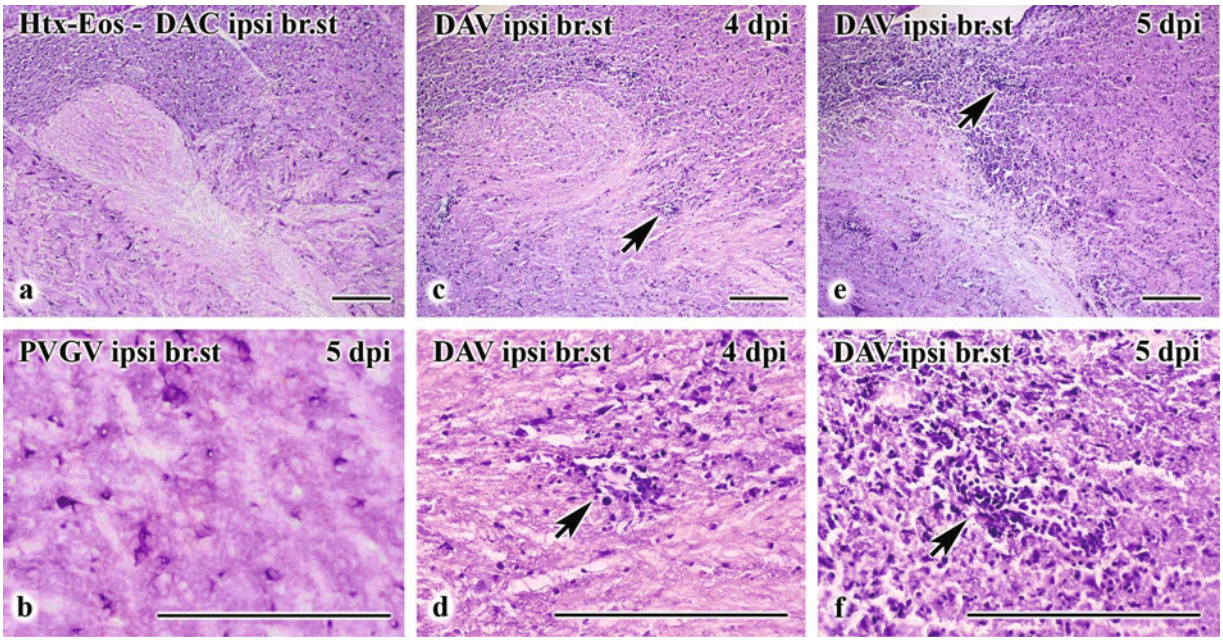

Figure 6 Inflammatory infiltrates are present in DA, but not PVG, rats. Kinetics of tissue inflammation after HSV-1 infection shown by HTX-Eos staining (HTX-Eos): (**a**) Brainstem of a control DA rat; (**b**) ipsilateral side of the brainstem of a PVG rat at 5 d.p.i. without inflammatory signs; (**c**) immune cell infiltrates (*arrow*) on the ipsilateral side of the brainstem of a DA rat at 4 d.p.i.; (**d**) higher magnification of section shown in (**c**), with perivascular infiltrate (*arrow*); (**e**) progression of inflammation in a DA rat at 5 d.p.i., with more widespread inflammatory infiltrates (*arrow*); (**f**) higher magnification of section shown in (**e**), with dense immune cell infiltrate (*arrow*). Scale bar = 200 μm.

numbers of ED1-positive cells in control PVG rats were slightly higher than in DA controls, but remained unchanged after inoculation (Figure 7f).

Recruitment of natural killer (NK) cells, as shown by immunolabeling for NK receptor, reached its peak by 5 d.p.i. in infected DA rats (Figure 7h). Only occasional NK cells were found in control DA (Figure 7g) and infected PVG rats (Figure 7i).

The first signs of CD4-positive perivascular infiltrates were seen at 3 d.p.i., with a peak at 5 d.p.i. (Figure 7k), and CD8-positive infiltrates could be observed at 4 d.p.i. (Figure 7m) in the brainstem of DA rats. By 5 d.p.i., a widespread distribution of CD4-positive and CD8-positive (Figure 7n) cells were seen throughout the parenchyma of the brainstem and cerebellum. In control animals (Figure 7j) and in HSV-1–infected PVG rats (Figure 7l, o), only occasional T cells were associated with blood vessels.

Immunohistochemical and histopathological data are summarized in Table 1.

Tissue damage and cell death

Apoptosis, an important feature of CNS injury in human HSE, was assessed by transferase-mediated dUTP nick-end labeling method (TUNEL). No TUNEL-positive cells were detected in control animals (Figure 8a). In inoculated DA rats, the first TUNEL-positive cells were detected at 3 d.p.i. on the ipsilateral side of the brainstem (Figure 8b), whereas 4 d.p.i. TUNEL-positive cells appeared on the contralateral side of the thalamus and in the cerebellum. Massive numbers of TUNEL-positive cells, indicating apoptotic cell death, were detected mainly on the ipsilateral side of the brainstem at 5 d.p.i. (Figure 8c, d) and even on the contralateral side of the thalamus (Figure 8e). Notably, TUNEL-positive cells were restricted mainly to areas of productive viral infection and inflammation and did not occur as a widespread or nonspecific process.

In HSV-1–infected PVG rats no TUNEL-positive cells could be detected (Figure 8f), except for the olfactory bulb, where only sporadic TUNEL-positive cells could be seen.

Discussion

It has proven to be difficult to create a representative model of HSE in adult rats, unless physically penetrating the blood-brain barrier by intraparenchymal (Engel *et al*, 2000) or intracerebroventricular (Ben-Hur *et al*, 2004; Weidenfeld *et al*, 2005) injections, or by injection of virus directly into the vagus nerve (Thompson *et al*, 2000). Yet another method has been nasal instillation targeting the olfactory nerve (Fujii *et al*, 1999; Garssen *et al*, 2000), a commonly used pathway in rodents to facilitate uptake into the brain compartment.

Here we describe a model of acute lethal HSE in inbred DA rats obtained by unilateral subcutaneous

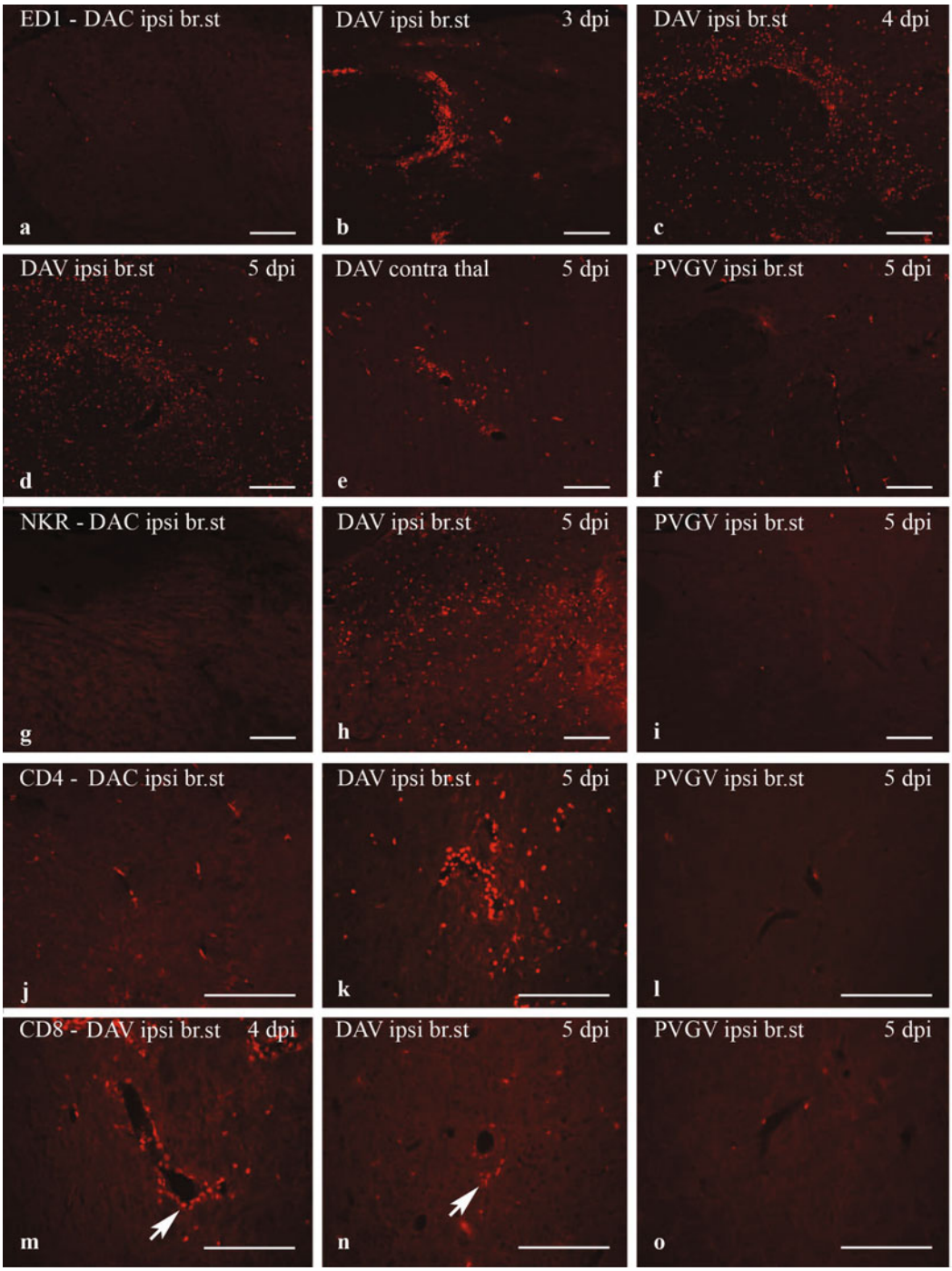

Figure 7 Immune cell infiltrates are present in HSV-1 infected DA, but not PVG rats. Recruitment of immune cells as a consequence of HSV-1 infection visualized by immunofluorescence staining for ED1 (phagocyting cells; **a–f**), NKR (NK cells; **g–i**), CD4 (helper T-cells; **j–l**), and CD8 (cytotoxic T cells; **m–o**): (**a**) Ipsilateral side of brainstem in control DA rat, without ED1–positive cells; (**b**) ipsilateral side of brainstem in DA rat at 3 d.p.i., with the first appearance of ED1–positive cells; (**c**) ipsilateral side of brainstem in DA rat at 4 d.p.i., with increased ED1 labeling; (**d**) ipsilateral side of brainstem in DA rat at 5 d.p.i., showing a massive presence of ED1–positive cells; (**e**) ED1–positive cells in the contralateral thalamic parenchyma of a DA rat at 5 d.p.i.; (**f**) ipsilateral side of brainstem in a PVG rat at 5 d.p.i., with a few ED1–positive cells associated with blood vessels; (**g**) NKR labeling in control DA rat devoid of immunoreactive cells; (**h**) massive recruitment of NK cells to the ipsilateral side of the brainstem of a DA rat at 5 d.p.i.; (**i**) ipsilateral side of brainstem of a PVG rat at 5 d.p.i., without signs of NK cell recruitment; (**j**) sporadic CD4-positive Tcells in the brainstem of a control DA rat; (**k**) massive perivascular infiltrate comprising numerous CD4-positive T cells on the ipsilateral side of the brainstem in a DA rat at 5 d.p.i.; (**l**) no CD4-positive T cells detectable on the ipsilateral side of the brainstem in a PVG rat at 5 d.p.i.; (**m**) perivascular infiltrate comprising CD8-positive T cells on the ipsilateral side of the brainstem of a DA rat at 4 d.p.i.; (**n**) ipsilateral side of the brainstem of a DA rat at 5 d.p.i., with parenchymal infiltration of CD8-positive cells; (**o**) ipsilateral side of the brainstem of a PVG rat at 5 d.p.i., with occasional CD8-positive cells. Scale bar = 200 μm.

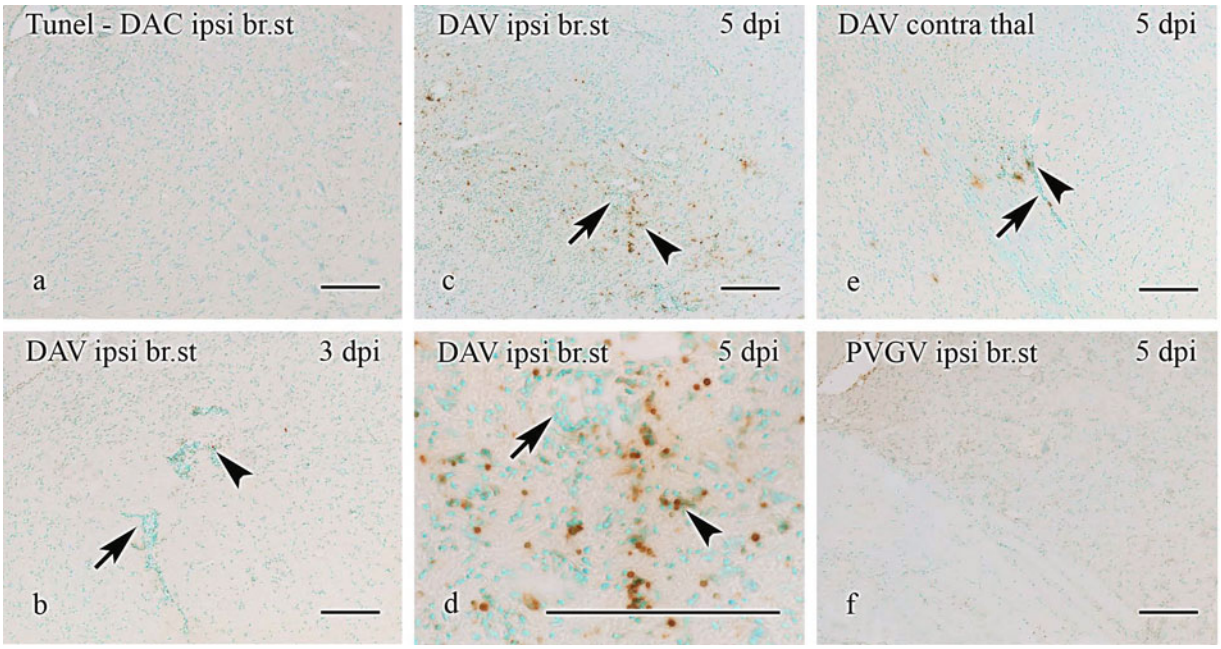

Figure 8 Evidence of apoptosis in HSV-1–infected DA, but not PVG, rats. Apoptosis as assessed by TUNEL staining in DA and PVG rats: (**a**) Ipsilateral side of brainstem in control DA rat, devoid of TUNEL labeling; (**b**) ipsilateral side of brainstem in DA rat at 3 d.p.i., with perivascular infiltrates (*arrow*) and a few TUNEL-positive cells (*arrowhead*); (**c**) ipsilateral side of brainstem in DA rat at 5 d.p.i., with massive immune cell infiltration (*arrow*) and numerous TUNEL-positive cells (*arrowhead*); (**d**) higher magnification of ipsilateral side of brainstem in DA rat at 5 d.p.i., with a perivascular infiltrate (*arrow*) and many TUNEL-positive cells (*arrowhead*); (**e**) contralateral side of the thalamus of DA rat at 5 d.p.i., with perivascular infiltrates (*arrow*) and TUNEL-positive cells (*arrowhead*); (**f**) ipsilateral side of brainstem in infected PVG rat at 5 d.p.i., devoid of TUNEL labeling. Scale bar = 200 μm.

injection of a brain biopsy–derived neurovirulent human HSV-1 strain into the right whiskers' area. DA rats developed neurological symptoms at 5 d.p.i., which rapidly progressed to acute, lethal encephalitis. The first histopathological changes appeared from 2 and 3 d.p.i. The onset and progression of clinical symptoms coincided with the histopathological findings, which were consistent with full-blown encephalitis mainly affecting the brainstem, thalamus, and cerebellum. Notably, all data from magnetic resonance imaging (MRI), histopathology, virus isolations, quantitative HSV-1 PCR assays, TUNEL staining for apoptosis, and H&E staining were concordant. If not euthanized, infected DA rats invariably die by the end of day 5 after inoculation as a result of the infection and the subsequent immunological reactions. Surprisingly, PVG rats of the same age as the DA rats, infected with the same or even higher doses of HSV-1, remain without clinical symptoms and histopathological alterations. There was no evidence that HSV-1 had penetrated into the CNS compartment. The notion of a failure in uptake or transport of HSV-1 in PVG rats is supported by the fact that virus could not be isolated in the trigeminal ganglia. As a possible explanation of this finding, a kinetic study of early events during the infection showed a more rapid clearance of HSV-1 in the whiskers area of PVG rats as compared to DA rats. The mechanisms behind this phenomenon remain to be elucidated, but we may speculate that DA rats show a less proficient innate immune response to HSV-1 infection than PVG rats do. Interestingly, a defect in oxidative capacity linked to genetic polymorphism within the NADPH oxidase complex and the β-interferon pathway was previously related to development of arthritis in this rat strain (Olofsson *et al*, 2003, 2007).

In the model presented here, HSV-1 reached the brainstem of the DA rats approximately 2 days following infection. From the entry zone, the virus spread along fiber tracts towards the thalamus, the cerebellum, and the contralateral side of the brainstem, starting a cascade of inflammatory responses, subsequently leading to dramatic encephalitis with fatal outcome (Figure 9a–d). By the choice of virus inoculation site, the encephalitic process started in the brainstem, but it propagated in rostral direction within short time. Interestingly, HSV-1 DNA as well as cellular markers of inflammation, such as MHC class II, ED1, and CD8, were demonstrable in the olfactory bulb, but also in other segments. Thus, in HSE the virus might spread either via the olfactory or the trigeminal route or by both.

Apoptosis, implicated in numerous acute and chronic neurological diseases, is also an important feature of virus-induced neuronal injury and death (Griffin and Hardwick, 1999; Mori *et al*, 2005; Thompson, 1995). Although the traditional view is that HSE pathology is characterized by a necrotizing

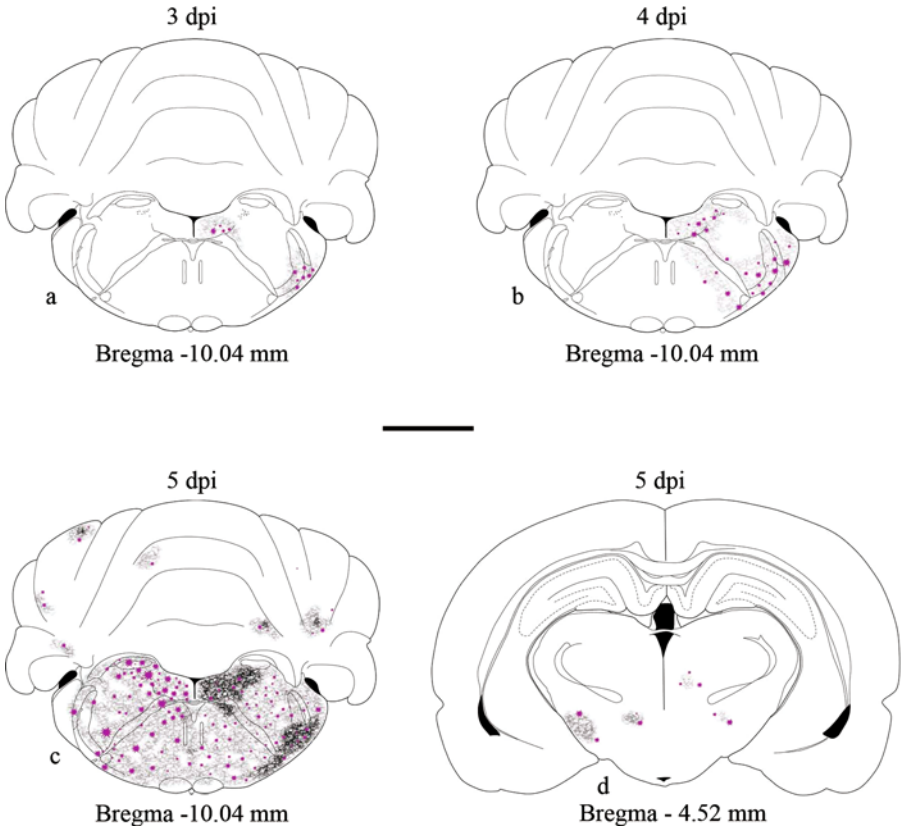

Figure 9 Schematic picture showing HSV-1 kinetics and consequent tissue and immune activation. Purple stars represent HSV-1, surrounding grey areas represent spread of tissue reaction, damage and inflammation. Scale bar = 2 mm.

process, there are numerous *in vitro* and *in vivo* studies emphasizing the apoptotic activity of HSV-1 in different cell types, including neurons and T cells (Geiger *et al*, 1997; Huang *et al*, 2005; Perkins *et al*, 2003; Pongpanich *et al*, 2004).

The results of this study support the occurrence of apoptotic cell death in regions of the brain affected by productive viral infection, with a magnitude that correlates to the concomitant inflammatory response. Thus, most TUNEL-positive cells at the earlier stages of infection were found in close proximity to perivascular infiltrates in the brainstem. As the infection propagates, apoptotic cells are encountered also in the parenchyma, suggesting that this might be a direct consequence of viral infection or bystander damage by immune cell activity. Further experimentation is needed to determine if apoptotic cells are of neuronal, glial, or T-cell origin. However, it seems likely that with such an acute disease course, most of the apoptotic cells are infiltrating immune cells and that nerve cells decay by necrosis. Nevertheless, during acute phase of HSE in humans, neuronal cells death is not exclusively necrotic, but a regulatory form of cell death, i.e., apoptosis, also occurs (DeBiasi *et al*, 2002). This stresses the need of identifying the mechanisms and the cell types involved in HSE-related neuronal damage, because this constitutes an important therapeutic target in parallel to viral suppression.

Prior studies have shown differences in susceptibility to HSE in various strains of mice (Ellison *et al*, 2000; Kastrukoff *et al*, 1986; Lopez, 1975) and in different ages (Johnson, 1964). Subsequent studies have suggested that the natural resistance, in particular of the C57BL/6 strain, rely on innate immune mechanisms with a relatively more enhanced interferon-α/β response. However, the study suggests that this mechanism only seems to provide a transient delay in HSV-1 infection and that there are no data in support of a fundamental difference in resistance to HSV-1 infection in mice (Halford *et al*, 2004). The role of the innate immune responses has been shown to be of importance in HSE type 1 (Johnson, 1964). Recently it has been shown that interferon responses are important for HSE type 1 in humans (Jouanguy *et al*, 2007; Zhang *et al*, 2007). Further studies are needed to determine if the differences in the susceptibility to HSE seen between DA and PVG are due to different interferon responses.

As previously mentioned, most studies in rats have employed invasive means of inoculation in outbred rat strains, such as Sprague-Dawley (Engel *et al*, 2000) or Wistar (Müller *et al*, 2005). In one single study, strain differences in ocular herpes infections

were examined and an increased susceptibility was observed in the Lewis rat and an intermediate sensitivity in the DA strain, whereas the PVG strain was resistant (Nicholls *et al*, 1994). The results obtained here corroborate and extend these data by demonstrating that variable resistance to HSV-1 infection is regulated at the level of entry into the nervous system. This suggests a more fundamental genetically regulated difference than what is proposed by prior mouse studies. The finding that clearance of the virus from the periphery differed in the two examined strains suggests that it may involve mechanisms related to the primary immune response. These results provide the basis for genetic mapping studies that can position the underlying genetic variations (Swanberg *et al*, 2005). Interestingly, support for the notion that susceptibility to HSE can be regulated by single traits has recently been obtained in humans (Casrouge *et al*, 2006). In two children, a deficiency in the intracellular protein UNC-93B, resulting in impaired interferon-α/β responses, was shown to be associated with increased susceptibility to HSE. This study suggests that variability in a single gene may confer susceptibility to specific pathogens without signs and symptoms of a general defect in the defense against infections.

In conclusion, we here describe a rat model of HSV-1 infection in which careful examination of the response in two inbred rat strains suggests the existence of a difference in susceptibility to HSE. In the resistant rat strain, virus entry into the nervous system was efficiently blocked, probably due to a rapid clearance of the peripheral infection, which in turn may be related to innate defense mechanisms. We have started experiments to position the gene or genes responsible for innate immune response to HSV-1, with possible bearings for host susceptibility to HSE. Furthermore, the here-described model can facilitate the dissection of important pathogenetic mechanisms of this severe medical condition.

Materials and methods

Animals

The experiments were carried out on inbred male Dark Agouti ($RT1^{av1}$) and Piebald Virol Glaxo ($RT1^{c}$) rats (Scanbur-BK AB, Sollentuna, Sweden). Twenty-five DA and 25 PVG rats were used for immunohistochemistry, 6 DA and 6 PVG for MRI, 15 DA and 15 PVG rats at 5 d.p.i. and 18 DA and 18 PVG rats for HSV-1 kinetic studies (12, 24, 48, 72, 96, 120 h) using qPCR and virus isolation. All rats were 45 days old when infected and analyzed at 1, 2, 3, 4 and 5 d.p.i. MRI was performed on the day prior to the infection (day −1), then 1, 3, and 5 d.p.i.

During the experiment, animals were kept in a full-barrier animal facility, at the Astrid Fagræus laboratory, within the Swedish Institute for Infectious Disease Control (SMI), in groups of 2 to 3 per cage under specific pathogen–free and climate-controlled conditions, with artificial 12-h light/dark cycles. The animals were housed in Eurotype IV polystyrene cages in enriched rat IVC (individually ventilated cage) system (Tecniplast, Italy) containing tin nests, aspen wood chips, aspen wood shavings, and aspen chew blocks (Tapvei, Finland), and fed standard rodent chow (SDS, England) and water *ad libitum*. Ambient temperature was 21°C. All experiments in this study were performed in accordance with the guidelines from the Swedish National Board for Laboratory Animals and the European Community Council Directive (86/609/EEC) and approved by the Swedish Ethical Committee (no.128/04).

Virus

HSV-1 virus strain I-2762 was isolated from a biopsy taken from a male patient on day 2 after onset of the first clinical symptoms of HSE. The patient died 2 days later as a consequence of the infection. The virus was propagated in green monkey kidney (GMK-AH1) cells for maximum two passages and was aliquoted and stored at −80°C. The isolate was typed as HSV-1 by enzyme-linked immunosorbent assay (ELISA) using type-specific monoclonal antibodies (mAbs) and infectivity titers were expressed in PFU/ml. In previous experimental studies, this strain showed a high degree of neurovirulence and neuroinvasiveness both *in vivo* and *in vitro* (Bergström *et al*, 1990; Bergström and Lycke, 1990). After being thawed to room temperature, 75 μl virus suspension containing 2×10^6 PFU HSV-1 was injected instantaneously s.c. into the area of the whiskers' base unilaterally, on the right side, under 2% isoflurane (Baxter) anesthesia.

Magnetic resonance imaging

Six DA and six PVG rats were infected at the age of 45 days. *In vivo* MRI investigations were performed in each rat at four different occasions, that is, 1 day prior to the infection (day −1) and 1, 3, and 5 days after infection (1, 3, 5 d.p.i.).

For the MRI, the rats were anesthetized using 1.0% to 2.0% isoflurane, which was delivered through a face mask and allowed for spontaneous respiration. The rats were investigated in supine position and the head was fixed by the upper incisives to an acrylic rig. Body temperature was recorded and maintained between 36.5°C and 37°C using an MRI-compatible air temperature control system. Respiratory rate was monitored continuously (BioTrigger; Bruker, Karlsruhe, Germany).

MRI examinations were performed using a 4.7-tesla magnet with horizontal bore (Bruker Biospec Avance 47/40; Bruker, Karlsruhe, Germany) equipped with a 12-cm inner diameter self-shielded gradient system. A commercially available circular resonator (Bruker) with an inner diameter of 35 mm was used for excitation and signal detection.

At each session a slice package of 11 frontal T2-weighted slices through the brain—slice thickness 1 mm, distance between two slices 2 mm (Figure 1e), field of view 30 mm, matrix 256 × 256, repetition time TR = 2566 ms, echo time TE = 30 ms, RARE factor 8 with RARE maximum 4, matrix size 256 × 256, and eight averages—was performed using spin echo sequences with rapid acquisition with relaxation enhancement (RARE) imaging (Hennig *et al*, 1986). The slice package was positioned with the 10th slice placed at the level of the rhinal fissure. In each MRI slice of each animal and time point, the grey intensity values were measured on the ipsi- and the contralateral side of the corresponding brain areas (Figure 1). The relative gray value (gray value of the area of interest on the ipsilateral side divided by the gray value of the contralateral side) on each slice was calculated and plotted against time. Spearman matrix, available to rank data, and Pearson matrix were calculated to detect a significant correlation between relative gray value and d.p.i., using appropriate software (SYSTAT, Evanston, IL, USA). Analysis was performed for all measured areas in DA and PVG rats.

Quantitative real-time PCR
Six DA and six PVG animals (five virus-infected and one control of each strain) were used for the qPCR reactions at 5 d.p.i.; 18 DA and 18 PVG rats were used for virus-kinetic studies (12, 24, 72, 96, and 120 h pi). The rats were perfused transcardiacally with 0.9% saline solution at 5 d.p.i. Samples were taken from the skin of the whiskers' base area, the trigeminal ganglia, brainstem, cerebellum, thalamus, cortex, and olfactory bulb from the ipsi- and contralateral sides. Samples from whiskers' area, brainstem and thalamus were divided into two pieces, one for qPCR and one for virus isolation experiments. All samples were kept in −80°C freezer for further processing.

DNA extraction was performed using the NucPrep Chemistry Isolation reagents (Applied Biosystems, Foster City, CA) according to the manufacturer's instructions.

A 118-nucleotide segment of the HSV-1 gB region was amplified by TaqMan PCR by use of HSV-1–specific forward primer (GCAGTTTACGTACAACCACATACAGC) HSV-1/2–specific reverse primer (AGCTTGCGGGCCTCGTT), and HSV-1–specific probe (CGGCCCAACATATCGTTGACATGGC), as described previously (Namvar *et al*, 2005). In brief, the reaction volume of 50 μl contained 25 μl universal master mix (Applied Biosystems), 10 μl of sample DNA, and primers and probes. Amplification was performed in an ABI Prism 7000 real-time PCR instrument (Applied Biosystems). After incubation for 2 min at 50°C (uracil-*N*-glycosylase digestion) and 10 min denaturation at 95°C, 45 cycles of two-step amplification (15 s at 95°C, 60 s at 58°C) were performed. As a standard for quantification of HSV-1 DNA, a dilution series of a plasmid (Gene Script) containing the targeted part of the gB-1 gene was included in each run. The DNA quantity of the plasmid was determined by spectrophotometry. From the resulting standard curve, the numbers of HSV-1 DNA copies as a function of Ct values were calculated.

Virus isolation
For the virus isolation experiment, thawed samples were homogenized in sterile physiological saline solution. For each sample, five tubes of GMK-AH1 cell cultures, cultured in Eagle's minimal essential medium supplemented with 2% calf serum and antibiotics, were infected, at a dilution scale of 10^{-1}, 10^{-2}, 10^{-3}, 10^{-4}, and 10^{-5}. Tubes were kept in a rotating culture chamber at 37°C and monitored daily for cytopathogenic effects by assessing infected cells during a period of 1 week. Virus isolation titers were given as the reciprocal value of the highest dilution yielding virus growth.

Exact Wilcoxon's two-sample test was used to assess the difference between the DA and the PVG rat strains with respect to number of DNA copies (qPCR) and viral load (virus isolation) after 5 d.p.i. for each of the different areas of measurement.

In the HSV-1 kinetic study, the number of DNA copies and viral load with respect to time after injection, in different areas of measurement in the two rat strains, was assessed by regression models. The dependent variables were log(1 + DNA copies) and log(1 + viral load), the explanatory variables were the rat strains, and time was set as a continuous variable, applying an interaction term between these variables. The *P* value for the interaction term showed whether the changes over time were different in the two strains.

Immunohistochemistry
The experiment was divided in two parts. In the acute HSE experiment, we used 20 rats. Five DA and five PVG rats were injected with virus, whereas five DA and five PVG control rats were injected by vehicle (Hanks' solution; Sigma-Aldrich, St. Louis, MO, USA) at 45 days of age. Brains were taken at 5 d.p.i. when all virus-infected DA rats had developed acute encephalitis.

In the experiment focused on the virus propagation and the subsequent development of the tissue and immunological reaction, we used an additional 30 rats. Of these, 10 DA rats and 10 PVG rats were infected with HSV-1 and 5 DA and 5 PVG control rats were injected with vehicle at 45 days of age. Two HSV-1–infected and one control rat of each strain were sacrificed at day 1, 2, 3, 4, and 5 d.p.i. Rats were anesthetized and perfused transcardiacally with 50 ml warm (37°C) saline solution, followed by 50 ml warm and then 200 ml cold fixative containing 4% paraformaldehyde and 0.4% picric acid in 0.16 M phosphate buffer (pH 6.9) (Pease, 1962; Zamboni, 1967). The brains were removed and immersed in the same fixative for 90 min and then cryoprotected

in 0.1 M phosphate buffer containing 10% sucrose, 0.02% sodiumazide (Sigma-Aldrich), and 0.01% bacitracin (Sigma). This procedure was carried out at the Astrid Fagræus Laboratory of the Swedish Institute for Infectious Disease Control (SMI) and thereafter the brains were processed at the Department of Clinical Neuroscience.

Coronal sections (14 μm thick) were cut at four levels of the brain, the olfactory bulb, frontal forebrain and striatum, hippocampal formation and thalamus, brainstem, and cerebellum (Bregma 6.70, 1.60, −4.52, and −10.04) (Paxinos and Watson, 1998) in a cryostat (Microm, Heidelberg, Germany) and thawed onto gelatin/chrome alum-coated microscope glass slides. The sections were processed for the indirect immunofluorescence staining (Coons, 1958).

Slides were covered with parafilm and incubated overnight in humidifying chambers at 4°C in the following primary antisera/antibodies diluted in phosphate-buffered saline (PBS) (pH 7.4) containing 0.3% Triton X-100 and 0.01% sodium azide (Sigma): polyclonal rabbit anti-human HSV-1 (Dako, Glostrup, Denmark) 1:100, for visualizing virus spread in the brain; polyclonal rabbit anti-cow glial fibrillary acidic protein (GFAP) (Dako) 1:100, to show the activation of astrocytes; mouse anti-rat OX-6 (Serotec, Oxford, UK) 1:200, to visualize microglial activation; mouse anti-rat CD68 (clone ED1) (Serotec) 1:200, to visualize phagocyting cells; mouse anti-rat CD4 (clone W3/25) (Serotec) 1:200, for staining of T cells; mouse anti-rat CD8 (kindly provided by Dr. Alan Williams, Oxford, UK) (Holmdahl *et al*, 1985) 1:200, to identify cytotoxic lymphocytes (CTLs); mouse anti-rat natural killer (NK) receptor (Harlan Sera-Lab, Loughborough, UK) 1:200, to visualize NK cells. After primary antibody incubation, slides were rinsed in PBS, incubated at 37°C for 40 min with Alexa Fluor 488–conjugated goat anti-rabbit secondary antibody 1:200 (Molecular Probes, Eugene, OR) (HSV-1 and GFAP), or with Cy-3–conjugated donkey anti-mouse (Jackson ImmunoResearch Laboratories, West Grove, PA, USA) secondary antibody 1:500 (OX-6, ED-1, CD4, CD8, NKR) in PBS containing 0.3% Triton X-100 and 0.01% sodium azide (Sigma). After rinsing, the slides were coverslipped with Mowiol (Calbiochem, La Jolla, CA, USA). The sections were analyzed under a Leica DM RBE microscope (Leica Microsystems AB, Sollentuna, Sweden). The specificity of the HSV-1 antiserum was tested by preabsorption with inactivated HSV-1 (I-2762), and remaining antisera/antibodies (earlier validated in our laboratory), by omission of the primary antibody.

Hematoxylin-eosin staining

Histological staining with Mayer's hematoxylin (Histolab Products AB, Gothenburg, Sweden) and eosin (Sigma-Aldrich) (H&E) was performed to visualize pathological changes and to reveal inflammatory infiltrations in the brain.

In situ TUNEL staining

The ApopTag Red *In Situ* Apoptosis Detection Kit (Chemicon International, CA, USA) was used for labeling of DNA fragments according to manufacturer's instructions. Cells were visualized using a light microscope for the presence of labeled nuclei as well as morphological changes associated with cells undergoing apoptosis. Cells were counterstained with Methyl Green (Sigma-Aldrich). A dark brown signal from diaminobenzidine indicated positive staining, whereas shades of blue-green signified nonreactive cells.

References

Aurelius E, Andersson B, Forsgren M, Sköldenberg B, Strannegard O (1994). Cytokines and other markers of intrathecal immune response in patients with herpes simplex encephalitis. *J Infect Dis* **170:** 678–681.

Aurelius E, Forsgren M, Sköldenberg B, Strannegard O (1993). Persistent intrathecal immune activation in patients with herpes simplex encephalitis. *J Infect Dis* **168:** 1248–1252.

Ben-Hur T, Itzik A, Barak O, Asher Y, Becker Y, Yirmiya R, Weidenfeld J (2004). Immunization with a nonpathogenic HSV-1 strain prevents clinical and neuroendocrine changes of experimental HSV-1 encephalitis. *J Neuroimmunol* **152:** 5–10.

Bergström T, Alestig K, Svennerholm B, Horal P, Sköldenberg B, Vahlne A (1990). Neurovirulence of herpes simplex virus types 1 and 2 isolates in diseases of the central nervous system. *Eur J Clin Microbiol Infect Dis* **9:** 751–757.

Bergström T, Lycke E (1990). Neuroinvasion by herpes simplex virus. An in vitro model for characterization of neurovirulent strains. *J Gen Virol* **71(Pt 2):** 405–410.

Booss J, Kim JH (1984). Biopsy histopathology in herpes simplex encephalitis and in encephalitis of undefined etiology. *Yale J Biol Med* **57:** 751–755.

Casrouge A, Zhang SY, Eidenschenk C, Jouanguy E, Puel A, Yang K, Alcais A, Picard C, Mahfoufi N, Nicolas N, Lorenzo L, Plancoulaine S, Senechal B, Geissmann F, Tabeta K, Hoebe K, Du X, Miller RL, Heron B, Mignot C, Billette de Villemeur T, Lebon P, Dulac O, Rozenberg F, Beutler B, Tardieu M, Abel L, Casanova JL (2006). Herpes simplex virus Encephalitis in human UNC-93B deficiency. *Science* **314:** 308–312.

Coons AH (1958). Fluorescent antibody methods. In: *General Cytochemical methods, Academic Press.* Danielli JF (ed.). New York**:** 399–422.

DeBiasi RL, Kleinschmidt-DeMasters BK, Richardson-Burns S, Tyler KL (2002). Central nervous system apoptosis in human herpes simplex virus and cytomegalovirus encephalitis. *J Infect Dis* **186:** 1547–1557.

Dijkstra CD, Dopp EA, Joling P, Kraal G (1985). The heterogeneity of mononuclear phagocytes in lymphoid

organs: distinct macrophage subpopulations in the rat recognized by monoclonal antibodies ED1, ED2 and ED3. *Immunology* **54:** 589–599.

Ellison AR, Yang L, Voytek C, Margolis TP (2000). Establishment of latent herpes simplex virus type 1 infection in resistant, sensitive, and immunodeficient mouse strains. *Virology* **268:** 17–28.

Engel JA, Zhang J, Bergström T, Conradi N, Forkstam C, Liljeroth A, Svensson L (2000). Neonatal herpes simplex virus type 1 brain infection affects the development of sensorimotor gating in rats. *Brain Res* **863:** 233–240.

Fujii S, Akaike T, Maeda H (1999). Role of nitric oxide in pathogenesis of herpes simplex virus encephalitis in rats. *Virology* **256:** 203–212.

Garssen J, van der Molen R, de Klerk A, Norval M, van Loveren H (2000). Effects of UV irradiation on skin and nonskin-associated herpes simplex virus infections in rats. *Photochem Photobiol* **72:** 645–651.

Geiger KD, Nash TC, Sawyer S, Krahl T, Patstone G, Reed JC, Krajewski S, Dalton D, Buchmeier MJ, Sarvetnick N (1997). Interferon-gamma protects against herpes simplex virus type 1-mediated neuronal death. *Virology* **238:** 189–197.

Griffin DE, Hardwick JM (1999). Perspective: virus infections and the death of neurons. *Trends Microbiol* **7:** 155–160.

Halford WP, Balliet JW, Gebhardt BM (2004). Re-evaluating natural resistance to herpes simplex virus type 1. *J Virol* **78:** 10086–10095.

Hennig J, Nauerth A, Friedburg H (1986). RARE imaging: a fast imaging method for clinical MR. *Magn Reson Med* **3:** 823–833.

Holmdahl R, Olsson T, Moran T, Klareskog L (1985). In vivo treatment of rats with monoclonal anti-T-cell antibodies. Immunohistochemical and functional analysis in normal rats and in experimental allergic neuritis. *Scand J Immunol* **22:** 157–169.

Huang CR, Lin SS, Chou MY, Ho CC, Wang L, Lee YL, Chen CS, Yang CC (2005). Demonstration of different modes of cell death upon herpes simplex virus 1 infection in different types of oral cells. *Acta Virol* **49:** 7–15.

Johnson RT (1964). The pathogenesis of herpes virus encephalitis: II. A cellular basis for the development of resistance with age. *J Exp Med* **120:** 359–374.

Jouanguy E, Zhang SY, Chapgier A, Sancho-Shimizu V, Puel A, Picard C, Boisson-Dupuis S, Abel L, Casanova JL (2007). Human primary immunodeficiencies of type I interferons. *Biochimie* **89:** 878–883.

Kastrukoff LF, Lau AS, Puterman ML (1986). Genetics of natural resistance to herpes simplex virus type 1 latent infection of the peripheral nervous system in mice. *J Gen Virol* **67(Pt 4):** 613–621.

Lidman O, Swanberg M, Horvath L, Broman KW, Olsson T, Piehl F (2003). Discrete gene loci regulate neurodegeneration, lymphocyte infiltration, and major histocompatibility complex class II expression in the CNS. *J Neurosci* **23:** 9817–9823.

Lopez C (1975). Genetics of natural resistance to herpesvirus infections in mice. *Nature* **258:** 152–153.

Lorentzen JC, Andersson M, Issazadeh S, Dahlman I, Luthman H, Weissert R, Olsson T (1997). Genetic analysis of inflammation, cytokine mRNA expression and disease course of relapsing experimental autoimmune encephalomyelitis in DA rats. *J Neuroimmunol* **80:** 31–37.

Lundberg C, Lidman O, Holmdahl R, Olsson T, Piehl F (2001). Neurodegeneration and glial activation patterns after mechanical nerve injury are differentially regulated by non-MHC genes in congenic inbred rat strains. *J Comp Neurol* **431:** 75–87.

Mori I, Goshima F, Mizuno T, Imai Y, Kohsaka S, Ito H, Koide N, Yoshida T, Yokochi T, Kimura Y, Nishiyama Y (2005). Axonal injury in experimental herpes simplex encephalitis. *Brain Res* **1057:** 186–190.

Müller AC, Maharaj H, Maharaj DS, Daya S (2005). Acyclovir protects against quinolinic-acid-induced oxidative neurotoxicity. *J Pharm Pharmacol* **57:** 883–888.

Namvar L, Olofsson S, Bergström T, Lindh M (2005). Detection and typing of herpes simplex virus (HSV) in mucocutaneous samples by TaqMan PCR targeting a gB segment homologous for HSV types 1 and 2. *J Clin Microbiol* **43:** 2058–2064.

Nicholls SM, Benylles A, Shimeld C, Easty DL, Hill TJ (1994). Ocular infection with herpes simplex virus in several strains of rat. *Invest Ophthalmol Vis Sci* **35:** 3260–3267.

Olofsson P, Holmberg J, Tordsson J, Lu S, Akerstrom B, Holmdahl R (2003). Positional identification of Ncf1 as a gene that regulates arthritis severity in rats. *Nat Genet* **33:** 25–32.

Olofsson P, Nerstedt A, Hultqvist M, Nilsson EC, Andersson S, Bergelin A, Holmdahl R (2007). Arthritis suppression by NADPH activation operates through an interferon-beta pathway. *BMC Biol* **5:** 19.

Paxinos G, Watson C (1998). *The rat brain in stereotaxic coordinates*, 4th ed. San Diego: Academic Press.

Pease PC (1962). Buffered formaldehyde as a killing agent and primary fixative for electron microscopy. *Anat Rec* **142:** 342.

Perkins D, Gyure KA, Pereira EF, Aurelian L (2003). Herpes simplex virus type 1-induced encephalitis has an apoptotic component associated with activation of c-Jun N-terminal kinase. *J NeuroVirol* **9:** 101–111.

Pongpanich A, Bhattarakosol P, Chirathaworn C (2004). Induction of apoptosis by herpes simplex virus in Jurkat cells is partly through caspase-3, -8 and -9 activation. *J Med Assoc Thai* **87(Suppl 2):** S140-S145.

Sabri F, Granath F, Hjalmarsson A, Aurelius E, Sköldenberg B (2006). Modulation of sFas indicates apoptosis in human herpes simplex encephalitis. *J Neuroimmunol* **171:** 171–176.

Sköldenberg B (1991). Herpes simplex encephalitis. *Scand J Infect Dis Suppl* **80:** 40–46.

Sköldenberg B, Aurelius E, Hjalmarsson A, Sabri F, Forsgren M, Andersson B, Linde A, Strannegard O, Studahl M, Hagberg L, Rosengren L (2006). Incidence and pathogenesis of clinical relapse after herpes simplex encephalitis in adults. *J Neurol* **253:** 163–170.

Sköldenberg B, Forsgren M, Alestig K, Bergström T, Burman L, Dahlqvist E, Forkman A, Fryden A, Lövgren K, Norlin K, Norrby R, Olding-Stenkvist E, de Vahl K (1984). Acyclovir versus vidarabine in herpes simplex encephalitis. Randomised multicentre study in consecutive Swedish patients. *Lancet* **2:** 707–711.

Studahl M, Rosengren L, Gunther G, Hagberg L (2000). Difference in pathogenesis between herpes simplex virus type 1 encephalitis and tick-borne encephalitis demonstrated by means of cerebrospinal fluid markers of glial and neuronal destruction. *J Neurol* **247:** 636–642.

Swanberg M, Lidman O, Padyukov L, Eriksson P, Åkesson E, Jagodic M, Lobell A, Khademi M, Börjesson O, Lindgren CM, Lundman P, Brookes AJ, Kere J, Luthman H, Alfredsson L, Hillert J, Klareskog L, Hamsten A, Piehl F, Olsson T (2005). MHC2TA is associated with differential MHC molecule expression and susceptibility to rheumatoid arthritis, multiple sclerosis and myocardial infarction. *Nat Genet* **37:** 486–494.

Thompson CB (1995). Apoptosis in the pathogenesis and treatment of disease. *Science* **267:** 1456–1462.

Thompson KA, Blessing WW, Wesselingh SL (2000). Herpes simplex replication and dissemination is not increased by corticosteroid treatment in a rat model of focal Herpes encephalitis. *J NeuroVirol* **6:** 25–32.

Weidenfeld J, Itzik A, Goshen I, Yirmiya R, Ben-Hur T (2005). Role of the central amygdala in modulating the pituitary-adrenocortical and clinical responses in experimental herpes simplex virus-1 encephalitis. *Neuroendocrinology* **81:** 267–272.

Weissert R, Wallström E, Storch MK, Stefferl A, Lorentzen J, Lassmann H, Linington C, Olsson T (1998). MHC haplotype-dependent regulation of MOG-induced EAE in rats. *J Clin Invest* **102:** 1265–1273.

Whitley RJ, Alford CA, Hirsch MS, Schooley RT, Luby JP, Aoki FY, Hanley D, Nahmias AJ, Soong SJ (1986). Vidarabine versus acyclovir therapy in herpes simplex encephalitis. *N Engl J Med* **314:** 144–149.

Zamboni IDM, C. (1967). Buffered picric acid formaldehyde. A new rapid fixative for electron microscopy. *J Cell Biol* **35:** 148A.

Zhang SY, Jouanguy E, Ugolini S, Smahi A, Elain G, Romero P, Segal D, Sancho-Shimizu V, Lorenzo L, Puel A, Picard C, Chapgier A, Plancoulaine S, Titeux M, Cognet C, von Bernuth H, Ku CL, Casrouge A, Zhang XX, Barreiro L, Leonard J, Hamilton C, Lebon P, Heron B, Vallee L, Quintana-Murci L, Hovnanian A, Rozenberg F, Vivier E, Geissmann F, Tardieu M, Abel L, Casanova JL (2007). TLR3 deficiency in patients with herpes simplex encephalitis. *Science* **317:** 1522–1527.